AIAA JOURNAL
Vol. 45, No. 12, December 2007

Closed-Form Solutions for Nonlinear Analysis of Single-Sided Bonded Composite Patch Repairs

Quantian Luo and Liyong Tong*
University of Sydney, Sydney, New South Wales 2006, Australia

DOI: 10.2514/1.30108

This paper presents novel analytical solutions for nonlinear analysis of single-sided adhesively bonded composite patch repairs to cracked structures in tension. In the present formulation, large deflections of adherends are taken into account in the equilibrium equations of the adhesively bonded patch repairs. In addition, large deflections of the overlap adherends, shear, and peel strains of the adhesive are included simultaneously in the derivation of the governing equations. By employing the boundary and continuity conditions, closed-form solutions are obtained for adherend displacements, adhesive stresses, and edge-moment factors for the repairs with isotropic adherends and composite adherends with symmetrical layups. The novel solutions are then simplified for practical uses. The geometrically nonlinear finite element analysis is conducted using MSC/NASTRAN. The numerical results predicted by the present closed-form solutions and their simplifications are compared with those of the nonlinear finite element analysis using MSC/NASTRAN. Remarkable agreement among the numerical results indicates that the present formulation and solutions are capable of capturing the geometrical nonlinearity of the single-sided bonded composite patch repairs to cracked structures.

I. Introduction

BONDED patch repair technology has been widely used to repair cracked thin-walled structures to extend their service life, because it can be used easily and can significantly enhance structural performance (Baker and Jones [1]). There are two types of bonded composite patch repairs to a cracked structure: single-sided and double-sided repairs. In practice, the single-sided bonded repair to a cracked structure is often used (Baker [2], Wang et al. [3], and Belhouari et al. [4]), because the double-sided repair may not be an option in the circumstances in which bonding access to the structure is only available from one side. To efficiently apply bonded repair technology, it is necessary to develop simple methods and formulas for conducting structural stress analysis for typical bonded repairs. The single-strap model shown in Fig. 1a is often used for studying a single-sided repair to a cracked plate subjected to a remote tension perpendicular to the crack. When the single-sided repair is supported in the overlap region, its stress analysis is similar to a double-sided repair or a double-strap joint. When there is no support in the overlap region, significantly large out-of-plane bending displacements in adherends have been observed (Klug and Sun [5] and Wang et al. [3]). In this case, structural stress analysis, particularly analytical stress analysis, becomes rather complex due to the factors such as geometrical nonlinearity, inaccurate stress prediction of laminates using classical beam theories, and fractures. Thus, geometrically nonlinear finite element analyses (NFEAs) have been widely used to take into account the important role of large deflections and to predict adhesive and adherend stresses (Chalkley and Baker [6], Osnes and Andersen [7], Oterkus et al. [8], and Kaye and Heller [9]).

In practical engineering design, simple and accurate analytical solutions are very useful and valuable becuase they can provide a fast estimate or benchmarking to structural performance, particularly in the preliminary design stage. To our best knowledge, closed-form nonlinear solutions for the single-strap model shown in Fig. 1a are not available in the open literature. In this paper, we present novel nonlinear analytical solutions for the single-strap model in Fig. 1a by extending the closed-form solutions for nonlinear analysis of single-lap bonded joints with isotropic adherends developed by Luo and Tong [10].

The present analytical solutions include closed-form formulas for edge-moment factors, adherend displacements, and adhesive stresses of the single-strap model shown in Fig. 1a. When these physical quantities are known, they can be used to calculate the energy release rate of cracked structures (Wang et al. [3]) and to study the debonding behavior of the bonded composite patch (Krenk [11] and Tong and Steven [12]).

The present solutions are obtained by assuming that the two composite adherends are identical and with symmetrical layups in the single-strap model shown in Fig. 1a. The derived solutions can be directly degenerated to the case of the single-strap model with isotropic adherends. The present solutions for the single-strap model in Fig. 1a with isotropic and composite adherends are validated by comparison with the numerical results of geometrically nonlinear finite element analyses using MSC/NASTRAN.

II. Analytical Solutions for the Model of Single-Sided Bonded Composite Patch Repairs

Consider the single-strap model shown in Fig. 1a. Adherends 1 and 2 are assumed to be identical, either isotropic or composite. For the case of composite adherends, the layup of each adherend is assumed to be symmetrical. To analyze the single-strap model in Fig. 1a, we subdivide the structure into four parts: O_1–I, I–II, II–$\bar{\text{I}}$, and $\bar{\text{I}}$–O_2. Because of the symmetry, only half of the model is required to be analyzed. In this paper, we consider the left half as shown in Fig. 1b.

A. Displacements of the Outer Adherend

In the coordinate system of Fig. 1b, displacements of the left outer adherend can be found:

$$u_3 = \frac{F}{A_{11}} x_3 + u_{o1}; \qquad w_3 = -\frac{M_{kl}}{F \sinh \beta_k l} \sinh \beta_k x_3 \tag{1}$$

where

$$\beta_k = \sqrt{\frac{F}{D_{11}}}$$

Received 29 January 2007; revision received 29 January 2007; accepted for publication 9 August 2007.

*School of Aerospace, Mechanical and Mechatronic Engineering; ltong@aeromech.usyd.edu.au (Corresponding Author).

It is noted the shear force Q is zero at cross sections O_1, O_2, and II due to symmetry. The solution procedure of Eq. (1) can be found in Luo and Tong [10]. In Eq. (1), u_{o1} denotes the axial displacement at point O_1, A_{11} and D_{11} are the tensional and bending stiffness of the composite adherend, F is the tensile force applied at points O_1 and O_2, and M_{kI} is the bending moment at cross section I, as shown in Fig. 1b. In Eq. (1), u_{o1} and M_{kI} are unknowns, which are to be determined by coupling with the displacements of the overlap.

B. Governing Equations of the Overlap Considering Large Deflections

To develop the governing equations, the following variables are introduced:

$$\begin{cases} 2u_s = u_2 + u_1; & 2w_s = w_2 - w_1; & 2u_a = u_2 - u_1; & 2w_a = w_2 + w_1 \\ 2N_s = N_2 + N_1; & 2Q_s = Q_2 - Q_1; & 2M_s = M_2 - M_1 \\ 2N_a = N_2 - N_1; & 2Q_a = Q_2 + Q_1; & 2M_a = M_2 + M_1 \end{cases} \tag{2}$$

The variables in Eq. (2) have the usual meanings, and subscripts 1 and 2 refer to adherends 1 and 2.

The constitutive equations of symmetrical composite beams for a general geometrical nonlinearity are

$$N = A_{11}\left[\frac{\mathrm{d}u}{\mathrm{d}x} + \frac{1}{2}\left(\frac{\mathrm{d}u}{\mathrm{d}x}\right)^2 + \frac{1}{2}\left(\frac{\mathrm{d}w}{\mathrm{d}x}\right)^2\right]; \qquad M = -D_{11}\frac{\mathrm{d}^2 w}{\mathrm{d}x^2} \tag{3}$$

The equilibrium equations for the free-body diagrams shown in Fig. 2 are

$$\begin{cases} \mathrm{d}N_1 + \tau(\mathrm{d}s_1)\frac{\mathrm{d}x}{\mathrm{d}s_1} = 0; & \mathrm{d}Q_1 + \sigma(\mathrm{d}x) + \tau\frac{\mathrm{d}w_1}{\mathrm{d}x}\,\mathrm{d}x = 0; & \mathrm{d}M_1 + \frac{t_1}{2}\tau(\mathrm{d}x) - Q_1\,\mathrm{d}x = -N_1\frac{\mathrm{d}w_1}{\mathrm{d}x}\,\mathrm{d}x \\ \mathrm{d}N_2 - \tau(\mathrm{d}s_2)\frac{\mathrm{d}x}{\mathrm{d}s_2} = 0; & \mathrm{d}Q_2 - \sigma(\mathrm{d}x) - \tau\frac{\mathrm{d}w_2}{\mathrm{d}x}\,\mathrm{d}x = 0; & \mathrm{d}M_2 + \frac{t_1}{2}\tau(\mathrm{d}x) - Q_2\,\mathrm{d}x = -N_2\frac{\mathrm{d}w_2}{\mathrm{d}x}\,\mathrm{d}x \end{cases} \tag{4}$$

where $(\mathrm{d}s_1)^2 = (\mathrm{d}x)^2 + (\mathrm{d}w_1)^2$ and $(\mathrm{d}s_2)^2 = (\mathrm{d}x)^2 + (\mathrm{d}w_2)^2$; t_1 is the adherend thickness; τ and σ are adhesive shear and peel stresses and are given by (Luo and Tong [10]):

$$\tau = \frac{2G_a}{t_a}\left(u_a + \frac{t_1}{2}\frac{\mathrm{d}w_a}{\mathrm{d}x}\right); \qquad \sigma = \frac{2E_a w_s}{t_a} \tag{5}$$

where E_a and G_a are Young's and shear moduli of the adhesive, and t_a is the adhesive thickness.

By using the variables defined in Eq. (2), the equilibrium equations become

$$\begin{cases} \frac{\mathrm{d}N_s}{\mathrm{d}x} = 0; \frac{\mathrm{d}Q_s}{\mathrm{d}x} - \sigma - \tau\frac{\mathrm{d}w_a}{\mathrm{d}x} = 0; & \frac{\mathrm{d}M_s}{\mathrm{d}x} - Q_s = -N_s\frac{\mathrm{d}w_s}{\mathrm{d}x} - N_a\frac{\mathrm{d}w_a}{\mathrm{d}x} \\ \frac{\mathrm{d}N_a}{\mathrm{d}x} - \tau = 0; \frac{\mathrm{d}Q_a}{\mathrm{d}x} - \tau\frac{\mathrm{d}w_s}{\mathrm{d}x} = 0; & \frac{\mathrm{d}M_a}{\mathrm{d}x} + \frac{t_1}{2}\tau - Q_a = -N_s\frac{\mathrm{d}w_a}{\mathrm{d}x} - N_a\frac{\mathrm{d}w_s}{\mathrm{d}x} \end{cases} \tag{6}$$

Equations (3), (5), and (6) include 12 variables: namely, six stress resultants and four displacements for the two adherends and two adhesive stress components. These equations are nonlinear differential equations and cannot be readily solved analytically. However, these full nonlinear governing equations can be converted into simplified nonlinear equations. Differentiating the third and sixth equations in Eq. (6), then substituting the second and fifth equations in Eq. (6), respectively, we have

$$\begin{cases} \frac{\mathrm{d}^2 M_s}{\mathrm{d}x^2} - \sigma - \tau\frac{\mathrm{d}w_a}{\mathrm{d}x} = -N_s\frac{\mathrm{d}^2 w_s}{\mathrm{d}x^2} - \frac{\mathrm{d}N_s}{\mathrm{d}x}\frac{\mathrm{d}w_s}{\mathrm{d}x} - N_a\frac{\mathrm{d}^2 w_a}{\mathrm{d}x^2} - \frac{\mathrm{d}N_a}{\mathrm{d}x}\frac{\mathrm{d}w_a}{\mathrm{d}x} \\ \frac{\mathrm{d}^2 M_a}{\mathrm{d}x^2} + \frac{t_1}{2}\frac{\mathrm{d}\tau}{\mathrm{d}x} - \tau\frac{\mathrm{d}w_s}{\mathrm{d}x} = -N_s\frac{\mathrm{d}^2 w_a}{\mathrm{d}x^2} - \frac{\mathrm{d}N_s}{\mathrm{d}x}\frac{\mathrm{d}w_a}{\mathrm{d}x} - N_a\frac{\mathrm{d}^2 w_s}{\mathrm{d}x^2} - \frac{\mathrm{d}N_a}{\mathrm{d}x}\frac{\mathrm{d}w_s}{\mathrm{d}x} \end{cases} \tag{7}$$

By noticing the first and fourth equations in Eq. (6), the third terms on the left-hand side and the fourth terms on the right-hand side of both equations in Eq. (7) cancel out, and the second terms on the right-hand side of both equations in Eq. (7) vanish. Noting that $N_s = \frac{1}{2}(N_1 + N_2) = \frac{1}{2}F$ and neglecting the following higher-order nonlinear terms,

$$\frac{\mathrm{d}u_a}{\mathrm{d}x}\frac{\mathrm{d}^2 w_s}{\mathrm{d}x^2}; \qquad \frac{\mathrm{d}u_a}{\mathrm{d}x}\frac{\mathrm{d}^2 w_a}{\mathrm{d}x^2} \tag{8}$$

we have the following equilibrium equations from Eqs. (6) and (7):

$$\begin{cases} \frac{\mathrm{d}N_s}{\mathrm{d}x} = 0; & \frac{\mathrm{d}^2 M_s}{\mathrm{d}x^2} - \sigma = -\frac{F}{2}\frac{\mathrm{d}^2 w_s}{\mathrm{d}x^2} \\ \frac{\mathrm{d}N_a}{\mathrm{d}x} - \tau = 0; & \frac{\mathrm{d}^2 M_a}{\mathrm{d}x^2} + \frac{t_1}{2}\frac{\mathrm{d}\tau}{\mathrm{d}x} = -\frac{F}{2}\frac{\mathrm{d}^2 w_a}{\mathrm{d}x^2} \end{cases} \tag{9}$$

In the definitions of adhesive shear and peel strains presented by Goland and Reissner [13], small strains and rotations of the adherends were assumed. To have a consistent formulation, we also neglect higher-order terms in Eq. (3). By using Eq. (2), the constitutive equations become

$$N_i = A_{11}\frac{\mathrm{d}u_i}{\mathrm{d}x}; \qquad M_i = -D_{11}\frac{\mathrm{d}^2 w_i}{\mathrm{d}x^2} \qquad (i = s, a) \tag{10}$$

By substituting Eqs. (5) and (10) into Eq. (9), the following governing equations in terms of displacements for the overlap region of the single-strap model in Fig. 1a are obtained:

$$\begin{cases} \frac{\mathrm{d}^2 u_s}{\mathrm{d}x^2} = 0 \\ D_{11}\frac{\mathrm{d}^4 w_s}{\mathrm{d}x^4} - \frac{F}{2}\frac{\mathrm{d}^2 w_s}{\mathrm{d}x^2} + \frac{2E_a}{t_a}w_s = 0 \end{cases} \tag{11}$$

$$\begin{cases} A_{11}\frac{\mathrm{d}^2 u_a}{\mathrm{d}x^2} - \frac{2G_a}{t_a}\left(u_a + \frac{t_1}{2}\frac{\mathrm{d}w_a}{\mathrm{d}x}\right) = 0 \\ -D_{11}\frac{\mathrm{d}^4 w_a}{\mathrm{d}x^4} + \frac{G_a t_1}{t_a}\left(\frac{\mathrm{d}u_a}{\mathrm{d}x} + \frac{t_1}{2}\frac{\mathrm{d}^2 w_a}{\mathrm{d}x^2}\right) + \frac{F}{2}\frac{\mathrm{d}^2 w_a}{\mathrm{d}x^2} = 0 \end{cases} \tag{12}$$

From a mathematical viewpoint, Eqs. (11) and (12) are linear differential equations for the given axial load F and can be analytically solved individually. The integration constants from both equations are coupled with each other and also with those for the displacements in sections O_1–I.

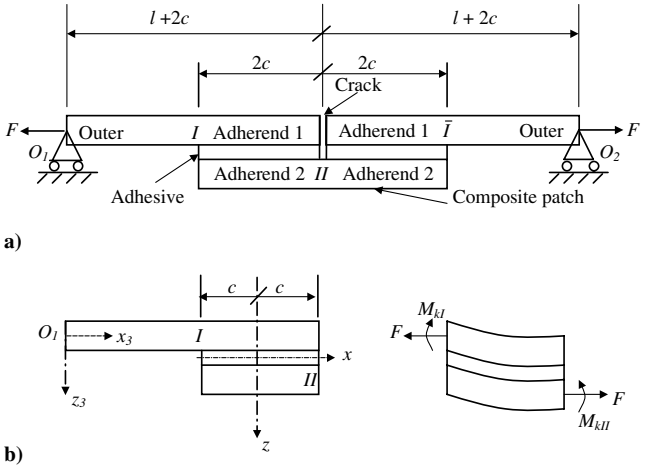

Fig. 1 Coordinate systems and force definitions of a single-sided bonded composite patch repair for a cracked structure.

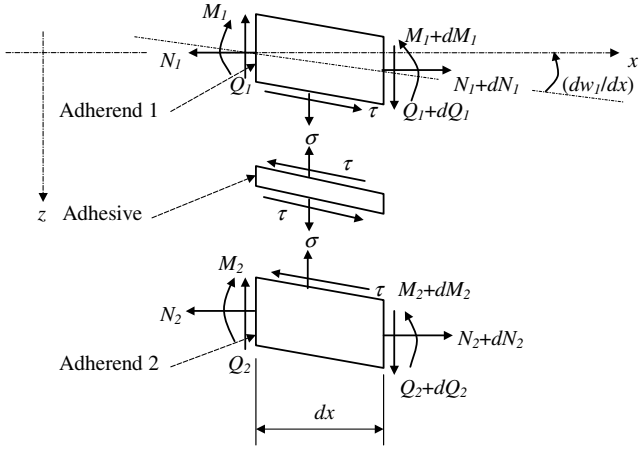

Fig. 2 Free-body diagrams of the overlap for geometrically nonlinear analysis.

According to Eq. (7), the retained nonlinear terms related to N_s (or F) reflect the role of large deflections in the equilibrium equations. Hence, the displacements determined from Eqs. (11) and (12) are nonlinearly dependent on the applied tensile loading F. A comparison between the present analytical solutions and the results obtained from the NFEAs using MSC/NASTRAN shows an extremely good correlation. This indicates that the present simplified nonlinear governing equation captures the critical features of geometric nonlinearity of the single-strap model in Fig. 1a.

The eigenvalues can be found by solving the characteristic equations and can be expressed as follows:

$$\begin{cases} \beta_{a1}^2 = \frac{1}{2}\left[\alpha_a\beta_\tau^2 + \frac{\beta_k^2}{2} + \sqrt{\alpha_a^2\beta_\tau^4 + \left(\alpha_a - \frac{1}{2}\right)\beta_\tau^2\beta_k^2 + \frac{\beta_k^4}{4}}\right] \\ \beta_{a2}^2 = \frac{1}{2}\left[\alpha_a\beta_\tau^2 + \frac{\beta_k^2}{2} - \sqrt{\alpha_a^2\beta_\tau^4 + \left(\alpha_a - \frac{1}{2}\right)\beta_\tau^2\beta_k^2 + \frac{\beta_k^4}{4}}\right] \end{cases} \tag{18}$$

C. Solutions of the Overlap Displacements

The closed-form solutions to Eq. (11) are

$$\begin{cases} u_s = A_{s1}x + A_{s2} \\ w_s = (B_{s1}\sinh\beta_{s1}x + B_{s2}\cosh\beta_{s1}x)\sin\beta_{s2}x + (B_{s3}\sinh\beta_{s1}x + B_{s4}\cosh\beta_{s1}x)\cos\beta_{s2}x \end{cases} \tag{13}$$

where A_{s1}, A_{s2}, and B_{si} $(i = 1, 2, 3, 4)$ are the integration constants, and the eigenvalues are

$$\beta_{s1} = \sqrt{\beta_\sigma^2 + \frac{\beta_k^2}{8}}; \qquad \beta_{s2} = \sqrt{\beta_\sigma^2 - \frac{\beta_k^2}{8}}; \qquad \beta_\sigma = \frac{\sqrt{2}}{2}\cdot\sqrt[4]{\frac{2E_a}{D_{11}t_a}} \tag{14}$$

The closed-form solutions to Eq. (12) are

$$\begin{cases} u_a = A_{a1}\sinh\beta_{a1}x + A_{a2}\cosh\beta_{a1}x + A_{a3}\sinh\beta_{a2}x + A_{a4}\cosh\beta_{a2}x + A_{a5} \\ w_a = B_{a1}\sinh\beta_{a1}x + B_{a2}\cosh\beta_{a1}x + B_{a3}\sinh\beta_{a2}x + B_{a4}\cosh\beta_{a1}x + B_{a5}x + B_{a6} \end{cases} \tag{15}$$

In Eq. (15), A_{ai} and B_{aj} $(i = 1, 2, \ldots, 5$ and $j = 1, 2, \ldots, 6)$ are the integration constants. They are not fully independent and their relationships are (Luo and Tong [10])

$$\begin{gathered} A_{a1} = K_{a1}B_{a2}; \qquad A_{a2} = K_{a1}B_{a1}; \qquad A_{a3} = K_{a2}B_{a4} \\ A_{a4} = K_{a2}B_{a3}; \qquad A_{a5} = -K_{a3}B_{a5} \end{gathered} \tag{16}$$

where

$$K_{a1} = \beta_{a1}K_{a10} = \frac{K_{a3}\beta_{a1}\beta_\tau^2}{4\beta_{a1}^2 - \beta_\tau^2}; \quad K_{a2} = \beta_{a2}K_{a20} = \frac{K_{a3}\beta_{a2}\beta_\tau^2}{4\beta_{a2}^2 - \beta_\tau^2} \qquad K_{a3} = \frac{t_1}{2} \tag{17}$$

where

$$\beta_\tau = \sqrt{\frac{8G_a}{A_{11}t_a}}; \qquad \alpha_a = \frac{1}{4}(1 + \alpha_k); \qquad \alpha_k = \frac{A_{11}t_1^2}{4D_{11}} \tag{19}$$

The composite coefficients α_a and α_k reflect the influence of ply layups of composite laminated adherends. For the isotropic materials, $\alpha_a = 1$ and $\alpha_k = 3$.

The integration constants in Eqs. (13) and (15) are determined, respectively, by using the following boundary conditions:

$$\begin{cases} x=-c\text{: } A_{11}\frac{\mathrm{d}u_s}{\mathrm{d}x}=\frac{F}{2}; & D_{11}\frac{\mathrm{d}^3w_s}{\mathrm{d}x^3}=\frac{F}{2}\frac{\mathrm{d}w_s}{\mathrm{d}x}; & D_{11}\frac{\mathrm{d}^2w_s}{\mathrm{d}x^2}=\frac{M_{k\mathrm{I}}}{2} \\ x=c\text{: } A_{11}\frac{\mathrm{d}u_s}{\mathrm{d}x}=\frac{F}{2}; & D_{11}\frac{\mathrm{d}^3w_s}{\mathrm{d}x^3}=\frac{F}{2}\frac{\mathrm{d}w_s}{\mathrm{d}x}; & D_{11}\frac{\mathrm{d}^2w_s}{\mathrm{d}x^2}=-\frac{M_{k\mathrm{II}}}{2} \end{cases} \tag{20}$$

$$\begin{cases} x=-c\text{: } A_{11}\frac{\mathrm{d}u_a}{\mathrm{d}x}=-\frac{F}{2}; & -D_{11}\frac{\mathrm{d}^3w_a}{\mathrm{d}x^3}+\frac{t_1\tau(-c)}{2}=-\frac{F}{2}\frac{\mathrm{d}w_a}{\mathrm{d}x}; & D_{11}\frac{\mathrm{d}^2w_a}{\mathrm{d}x^2}=-\frac{M_{k\mathrm{I}}}{2} \\ x=c\text{: } A_{11}\frac{\mathrm{d}u_a}{\mathrm{d}x}=\frac{F}{2}; & -D_{11}\frac{\mathrm{d}^3w_a}{\mathrm{d}x^3}+\frac{t_1\tau(c)}{2}=-\frac{F}{2}\frac{\mathrm{d}w_a}{\mathrm{d}x}; & D_{11}\frac{\mathrm{d}^2w_a}{\mathrm{d}x^2}=-\frac{M_{k\mathrm{II}}}{2} \end{cases} \tag{21}$$

In Eqs. (20) and (21), $M_{k\mathrm{I}}$ and $M_{k\mathrm{II}}$ are the edge moments at cross sections I and II, as shown in Fig. 1b. It is noted that the shear force Q is perpendicular to axis x, which is different from the shear force in the deformed-beam cross section.

Substituting Eq. (13) into Eq. (20), we have

$$A_{s1}=\frac{F}{2A_{11}} \tag{22}$$

$$\begin{cases} B_{s1}F_1''(c)+B_{s4}F_4''(c)=-\frac{M_{k\mathrm{II}}-M_{\mathrm{I}}}{4D_{11}} \\ B_{s1}[2F_1'''(c)-\beta_k^2F_1'(c)]+B_{s4}[2F_4'''(c)-\beta_k^2F_4'(c)]=0 \end{cases} \tag{23}$$

$$\begin{cases} B_{s2}F_2''+B_{s3}F_3''=-\frac{M_{k\mathrm{II}}+M_{k\mathrm{I}}}{4D_{11}} \\ B_{s2}[2F_2'''(c)-\beta_k^2F_2'(c)]+B_{s3}[2F_3'''(c)-\beta_k^2F_3'(c)]=0 \end{cases} \tag{24}$$

In Eqs. (23) and (24), F_i', F_i'', and F_i''' ($i=1, 2, 3, 4$) are the first-, second-, and third-order derivatives of the following functions:

$$\begin{cases} F_1(x)=\sinh\beta_{s1}x\sin\beta_{s2}x; & F_2(x)=\cosh\beta_{s1}x\sin\beta_{s2}x \\ F_3(x)=\sinh\beta_{s1}x\cos\beta_{s2}x; & F_4(x)=\cosh\beta_{s1}x\cos\beta_{s2}x \end{cases} \tag{25}$$

Solving Eqs. (23) and (24), we have

$$\begin{cases} B_{s1}=b_{sM1}(M_{k\mathrm{II}}-M_{k\mathrm{I}}); & B_{s4}=b_{sM4}(M_{k\mathrm{II}}-M_{k\mathrm{I}}) \\ B_{s2}=b_{sM2}(M_{k\mathrm{II}}+M_{k\mathrm{I}}); & B_{s3}=b_{sM3}(M_{k\mathrm{II}}+M_{k\mathrm{I}}) \end{cases} \tag{26}$$

where

$$\begin{cases} b_{sM1}=-\frac{[2F_4'''(c)-\beta_k^2F_4'(c)]}{4D_{11}\{[2F_4'''(c)-\beta_k^2F_4'(c)]F_1''(c)-[2F_1'''(c)-\beta_k^2F_1'(c)]F_4''(c)\}} \\ b_{sM4}=\frac{[2F_1'''(c)-\beta_k^2F_1'(c)]}{4D_{11}\{[2F_4'''(c)-\beta_k^2F_4'(c)]F_1''(c)-[2F_1'''(c)-\beta_k^2F_1'(c)]F_4''(c)\}} \\ b_{sM2}=-\frac{[2F_3'''(c)-\beta_k^2F_3'(c)]}{4D_{11}\{[2F_3'''(c)-\beta_k^2F_3'(c)]F_2''(c)-[2F_2'''(c)-\beta_k^2F_2'(c)]F_3''(c)\}} \\ b_{sM3}=\frac{[2F_2'''(c)-\beta_k^2F_2'(c)]}{4D_{11}\{[2F_3'''(c)-\beta_k^2F_3'(c)]F_2''(c)-[2F_2'''(c)-\beta_k^2F_2'(c)]F_3''(c)\}} \end{cases} \tag{27}$$

Substituting Eq. (15) into Eq. (21) and noting Eqs. (16) and (17), we have

$$\begin{cases} (K_{a10}\beta_{a1}^2\cosh\beta_{a1}c)B_{a2}+(K_{a20}\beta_{a2}^2\cosh\beta_{a2}c)B_{a4}=0 \\ (\beta_{a1}^2\cosh\beta_{a1}c)B_{a2}+(\beta_{a2}^2\cosh\beta_{a2}c)B_{a4}=-\frac{M_{k\mathrm{II}}+M_{k\mathrm{I}}}{4D_{11}} \end{cases} \tag{28}$$

$$\begin{cases} (K_{a10}\beta_{a1}^2\sinh\beta_{a1}c)B_{a1}+(K_{a20}\beta_{a2}^2\sinh\beta_{a2}c)B_{a3}=\frac{F}{2A_{11}} \\ (\beta_{a1}^2\sinh\beta_{a1}c)B_{a1}+(\beta_{a2}^2\sinh\beta_{a2}c)B_{a3}=-\frac{M_{k\mathrm{II}}-M_{k\mathrm{I}}}{4D_{11}} \end{cases} \tag{29}$$

The integration constants B_{ai} ($i=1, 2, 3, 4$) can be expressed as

$$\begin{cases} B_{a1}=b_{aF1}+b_{aM1}(M_{k\mathrm{II}}-M_{k\mathrm{I}}); & B_{a3}=b_{aF3}+b_{aM3}(M_{k\mathrm{II}}-M_{k\mathrm{I}}) \\ B_{a2}=b_{aM2}(M_{k\mathrm{II}}+M_{k\mathrm{I}}); & B_{a4}=b_{aM4}(M_{k\mathrm{II}}+M_{k\mathrm{I}}) \end{cases} \tag{30}$$

where

$$\begin{cases} b_{aF1}=\frac{F}{2A_{11}\beta_{a1}^2(K_{a10}-K_{a20})\sinh\beta_{a1}c}; & b_{aM1}=\frac{K_{a20}}{4D_{11}\beta_{a1}^2(K_{a10}-K_{a20})\sinh\beta_{a1}c} \\ b_{aF3}=\frac{F}{2A_{11}\beta_{a2}^2(K_{a20}-K_{a10})\sinh\beta_{a2}c}; & b_{aM3}=\frac{K_{a10}}{4D_{11}\beta_{a2}^2(K_{a20}-K_{a10})\sinh\beta_{a2}c} \\ b_{aM2}=\frac{K_{a20}}{4D_{11}\beta_{a1}^2(K_{a10}-K_{a20})\cosh\beta_{a1}c}; & b_{aM4}=\frac{K_{a10}}{4D_{11}\beta_{a2}^2(K_{a20}-K_{a10})\cosh\beta_{a2}c} \end{cases} \tag{31}$$

The displacements of sections II–$\bar{\mathrm{I}}$ and $\bar{\mathrm{I}}$–O_2 can be obtained in a similar manner because of the existence of symmetry in the single-strap model shown in Fig. 1a.

In Eqs. (13) and (15), the integration constants A_{s2}, B_{a5} (or A_{a5}), B_{a6}, $M_{k\mathrm{I}}$, and $M_{k\mathrm{II}}$ have not yet been determined because they are coupled with the displacements of the outer adherend and the symmetry conditions at cross section II.

D. Closed-Form Solutions of Edge Moments and Adhesive Stresses

There are six unknown constants: namely, u_{o1}, A_{s2}, B_{a5} (or A_{a5}), B_{a6}, $M_{k\mathrm{I}}$, and $M_{k\mathrm{II}}$ in Eqs. (1), (13), and (15). These unknown constants must be determined by considering the continuity conditions at cross sections I and II.

The displacement and slope continuity conditions of adherend 1 at cross section I can be imposed by the following equations:

$$\begin{aligned} \frac{Fl}{A_{11}}+u_{o1}=&-\frac{Fc}{2A_{11}}+A_{s2}-[K_{a1}(B_{a1}\cosh\beta_{a1}c-B_{a2}\sinh\beta_{a1}c) \\ &+K_{a2}(B_{a3}\cosh\beta_{a2}c-B_{a4}\sinh\beta_{a2}c)-K_{a3}B_{a5}] \end{aligned} \tag{32}$$

$$\begin{aligned} -\frac{M_{k\mathrm{I}}}{F}=&(-B_{a1}\sinh\beta_{a1}c+B_{a2}\cosh\beta_{a1}c-B_{a3}\sinh\beta_{a2}c \\ &+B_{a4}\cosh\beta_{a1}c-B_{a5}c+B_{a6}) \\ &-[B_{s1}F_1(c)-B_{s2}F_2(c)-B_{s3}F_3(c)+B_{s4}F_4(c)] \end{aligned} \tag{33}$$

$$\begin{aligned} -\frac{M_{k\mathrm{I}}\beta_k\coth\beta_kl}{F}=&\beta_{a1}(B_{a1}\cosh\beta_{a1}c-B_{a2}\sinh\beta_{a1}c) \\ &+\beta_{a2}(B_{a3}\cosh\beta_{a2}c-B_{a4}\sinh\beta_{a2}c)+B_{a5} \\ &-[-B_{s1}F_1'(c)+B_{s2}F_2'(c)+B_{s3}F_3'(c)-B_{s4}F_4'(c)] \end{aligned} \tag{34}$$

Because cross section II is a symmetric plane for adherend 2, as shown in Fig. 1a, we have the following symmetrical conditions for the displacements of adherend 2:

$$[K_{a1}(B_{a1}\cosh\beta_{a1}c + B_{a2}\sinh\beta_{a1}c) + K_{a2}(B_{a3}\cosh\beta_{a2}c + B_{a4}\sinh\beta_{a2}c) - K_{a3}B_{a5}] + \frac{Fc}{2A_{11}} + A_{s2} = 0 \tag{35}$$

$$\beta_{a1}(B_{a1}\cosh\beta_{a1}c + B_{a2}\sinh\beta_{a1}c) + \beta_{a2}(B_{a3}\cosh\beta_{a2}c + B_{a4}\sinh\beta_{a2}c) + B_{a5} + [B_{s1}F_1'(c) + B_{s2}F_2'(c) + B_{s3}F_3'(c) + B_{s4}F_4'(c)] = 0 \tag{36}$$

$$M_{k\mathrm{II}} = -F[(t_1 + t_a) + w_2(c)] \tag{37}$$

The six unknowns u_{o1}, A_{s2}, B_{a5} (or A_{a5}), $B_{a6}, M_{k\mathrm{I}}$, and $M_{k\mathrm{II}}$ in Eqs. (1), (13), and (15) can now be uniquely determined by solving Eqs. (32–37). The edge moments $M_{k\mathrm{I}}$ and $M_{k\mathrm{II}}$ at cross sections I and II, as shown in Fig. 1b, can be determined and expressed as

$$M_{k\mathrm{I}} = \frac{a_{22}b_1}{a_{11}a_{22} - a_{21}a_{12}}; \qquad M_{k\mathrm{II}} = -\frac{a_{21}b_1}{a_{11}a_{22} - a_{21}a_{12}} \tag{38}$$

where

$$\begin{cases} a_{11} = 1 + 2F\{(b_{aM1}\sinh\beta_{a1}c + b_{aM3}\sinh\beta_{a2}c) + [b_{sM1}F_1(c) + b_{sM4}F_4(c)]\} + 2cF\{\beta_{a1}(-b_{aM1}\cosh\beta_{a1}c + b_{aM2}\sinh\beta_{a1}c) \\ \quad +\beta_{a2}(-b_{aM3}\cosh\beta_{a2}c + b_{aM4}\sinh\beta_{a2}c) + [-b_{sM1}F_1'(c) + b_{sM2}F_2'(c) + b_{sM3}F_3'(c) - b_{sM4}F_4'(c)]\} \\ a_{12} = -1 - 2F\{(b_{aM1}\sinh\beta_{a1}c + b_{aM3}\sinh\beta_{a2}c) + [b_{sM1}F_1(c) + b_{sM4}F_4(c)]\} + 2cF\{\beta_{a1}(b_{aM1}\cosh\beta_{a1}c + b_{aM2}\sinh\beta_{a1}c) \\ \quad +\beta_{a2}(b_{aM3}\cosh\beta_{a2}c + b_{aM4}\sinh\beta_{a2}c) + [b_{sM1}F_1'(c) + b_{sM2}F_2'(c) + b_{sM3}F_3'(c) + b_{sM4}F_4'(c)]\} \\ a_{21} = \beta_k\coth\beta_k l - 2F[(\beta_{a1}b_{aM2}\sinh\beta_{a1}c + \beta_{a2}b_{aM4}\sinh\beta_{a2}c) + b_{sM2}F_2'(c) + b_{sM3}F_3'(c)] \\ a_{22} = -2F[(\beta_{a1}b_{aM2}\sinh\beta_{a1}c + \beta_{a2}b_{aM4}\sinh\beta_{a2}c) + b_{sM2}F_2'(c) + b_{sM3}F_3'(c)] \\ b_1 = F\{(t_1 + t_a) + 2[b_{aF1}(\sinh\beta_{a1}c - \beta_{a1}c\cosh\beta_{a1}c) + b_{aF3}(\sinh\beta_{a2}c - \beta_{a2}c\cosh\beta_{a2}c)]\} \end{cases} \tag{39}$$

When the edge moments $M_{k\mathrm{I}}$ and $M_{k\mathrm{II}}$ are known, the integration constants B_{a5}, A_{s2}, B_{a6}, and u_{o1} can be determined subsequently from Eqs. (32), (33), (36), and (38). Hence, we can determine the six unknown integration constants u_{o1}, A_{s2}, B_{a5} (or A_{a5}), B_{a6}, $M_{k\mathrm{I}}$, and $M_{k\mathrm{II}}$ in Eqs. (1), (13), and (15).

Similar to the case for the single-lap joints, we introduce the following edge-moment factors to depict nonlinear characteristics for the single-strap model shown in Fig. 1a:

$$k_{\mathrm{I}} = \frac{M_{k\mathrm{I}}}{F(t_1 + t_a)}; \qquad k_{\mathrm{II}} = -\frac{M_{k\mathrm{II}}}{F(t_1 + t_a)} \tag{40}$$

For the case of linear analysis, $k_{\mathrm{I}} = 0$ and $k_{\mathrm{II}} = 1$.

Noting Eq. (5), the adhesive shear and peel stresses can be determined:

$$\begin{cases} \tau = \frac{2G_a}{t_a}\left[\frac{2t_1\beta_{a1}^3}{4\beta_{a1}^2 - \beta_\tau^2}(B_{a1}\cosh\beta_{a1}x + B_{a2}\sinh\beta_{a1}x) + \frac{2t_1\beta_{a2}^3}{4\beta_{a2}^2 - \beta_\tau^2}(B_{a3}\cosh\beta_{a2}x + B_{a4}\sinh\beta_{a2}x)\right] \\ \sigma = \frac{2E_a}{t_a}[(B_{s1}\sinh\beta_{s1}x + B_{s2}\cosh\beta_{s1}x)\sin\beta_{s2}x + (B_{s3}\sinh\beta_{s1}x + B_{s4}\cosh\beta_{s1}x)\cos\beta_{s2}x] \end{cases} \tag{41}$$

The preceding expressions for the edge-moment factors, displacements, and adhesive stresses are complex, and simplified formulations without losing precision are important and necessary.

III. Simplification of Edge-Moment Factors, Adhesive Stresses, and Overlap Deflections

To simplify the analytical solutions in Eqs. (13), (15), and (38–41), we use the following approximations:

$$\begin{cases} \sinh\beta_{s1}c \approx \cosh\beta_{s1}c \approx \frac{e^{\beta_{s1}c}}{2}; \qquad \sinh\beta_{s2}c \approx \cosh\beta_{s2}c \approx \frac{e^{\beta_{s2}c}}{2}; \qquad \sinh\beta_{a1}c \approx \cosh\beta_{a1}c \approx \frac{e^{\beta_{a1}c}}{2} \\ \beta_{s1} \approx \beta_{s2} \approx \beta_\sigma; \qquad 4\beta_\sigma^2 \gg \beta_k^2 \end{cases} \tag{42}$$

By using Eqs. (40) and (42), the expressions of the integration constants can be simplified as

$$\begin{cases} B_{s1} = \frac{(k_{\mathrm{II}} + k_{\mathrm{I}})(t_1 + t_a)\beta_k^2(\cos\beta_{s2}c + \sin\beta_{s2}c)}{4\beta_\sigma^2\sinh\beta_{s1}c} \\ B_{s4} = -\frac{(k_{\mathrm{II}} + k_{\mathrm{I}})(t_1 + t_a)\beta_k^2(\cos\beta_{s2}c - \sin\beta_{s2}c)}{4\beta_\sigma^2 D_{11}\sinh\beta_{s1}c} \\ B_{s2} = \frac{(k_{\mathrm{II}} - k_{\mathrm{I}})(t_1 + t_a)\beta_k^2(\cos\beta_{s2}c + \sin\beta_{s2}c)}{4\beta_\sigma^2 D_{11}\sinh\beta_{s1}c} \\ B_{s3} = -\frac{(k_{\mathrm{II}} - k_{\mathrm{I}})(t_1 + t_a)\beta_k^2(\cos\beta_{s2}c - \sin\beta_{s2}c)}{4\beta_\sigma^2 D_{11}\sinh\beta_{s1}c} \end{cases} \tag{43}$$

$$\begin{cases} B_{a1} = \frac{t_1(4\beta_{a1}^2-\beta_\tau^2)\beta_k^2}{16\beta_{a1}^2(\beta_{a2}^2-\beta_{a1}^2)\sinh\beta_{a1}c}\left[\frac{4\beta_{a2}^2-\beta_\tau^2}{\alpha_k\beta_\tau^2}-(k_{\rm II}+k_{\rm I})(1+t_a/t_1)\right] \\ B_{a3} = \frac{t_1(4\beta_{a2}^2-\beta_\tau^2)\beta_k^2}{16\beta_{a2}^2(\beta_{a1}^2-\beta_{a2}^2)\sinh\beta_{a2}c}\left[\frac{4\beta_{a1}^2-\beta_\tau^2}{\alpha_k\beta_\tau^2}-(k_{\rm II}+k_{\rm I})(1+t_a/t_1)\right] \\ B_{a2} = -\frac{(4\beta_{a1}^2-\beta_\tau^2)\beta_k^2(k_{\rm II}-k_{\rm I})(t_1+t_a)}{16\beta_{a1}^2(\beta_{a2}^2-\beta_{a1}^2)\cosh\beta_{a1}c}; \qquad B_{a4} = -\frac{(4\beta_{a2}^2-\beta_\tau^2)\beta_k^2(k_{\rm II}-k_{\rm I})(t_1+t_a)}{16\beta_{a2}^2(\beta_{a1}^2-\beta_{a2}^2)\cosh\beta_{a2}c} \\ B_{a5} = -[\beta_{a1}B_{a1}\cosh\beta_{a1}c+\beta_{a2}B_{a3}\cosh\beta_{a2}c]-\frac{\beta_k(t_1+t_a)}{4\beta_\sigma}[\beta_k k_{\rm II}+k_{\rm I}(\beta_k+2\beta_\sigma\coth\beta_k l)] \\ B_{a6} = B_{a1}\sinh\beta_{a1}c-B_{a2}\cosh\beta_{a1}c+B_{a3}\sinh\beta_{a2}c-B_{a4}\cosh\beta_{a1}c+B_{a5}c-k_{\rm I}(t_1+t_a) \end{cases} \tag{44}$$

Our numerical computations show that the relation $w_s \ll w_a$ holds for most cases. Therefore, the simplified adherend deflections in the overlap are

$$w_1 \approx w_2 \approx w_a = B_{a1}\sinh\beta_{a1}x + B_{a2}\cosh\beta_{a1}x + B_{a3}\sinh\beta_{a2}x + B_{a4}\cosh\beta_{a1}x + B_{a5}x + B_{a6} \tag{45}$$

where the simplified integration constants are given in Eq. (44). It is worth noting that the approximation $w_1 \approx w_2 \approx w_a$ can only be used in the final approximate solution and must not be used in the derivation process; otherwise, the peel stress effect is ignored.

When the edge-moment factors are determined, the simplified adhesive stresses can be obtained by Eqs. (41), (43), and (44), and the deflections can be calculated by Eqs. (1) and (45).

To further simplify the edge-moment factors, we use the following approximation:

$$\beta_{a1} \approx \alpha_a\beta_\tau \gg \beta_{a2} \tag{46}$$

By using Eqs. (39), (40), (42), and (46), the simplified edge-moment factors can be expressed as

$$k_{\rm I} = \frac{\Delta_b\Delta_{22}}{\Delta_{11}\Delta_{22}-\Delta_{12}\Delta_{21}}; \qquad k_{\rm II} = -\frac{\Delta_b\Delta_{21}}{\Delta_{11}\Delta_{22}-\Delta_{12}\Delta_{21}} \tag{47}$$

where

$$\begin{cases} \Delta_{11} = 1-\frac{\beta_k^2}{8\alpha_a\beta_{a2}^2}\left(1-\frac{2\beta_{a2}c}{\sinh 2\beta_{a2}c}\right)-\frac{\beta_k^2}{4\beta_\sigma^2}; \qquad \Delta_{12} = 1-\frac{\beta_k^2}{8\alpha_a\beta_{a2}^2}\left(1-\frac{2\beta_{a2}c}{\tanh 2\beta_{a2}c}\right)+\frac{\alpha_k\beta_k^2c}{4\alpha_a\beta_{a1}}+\frac{\beta_k^2c}{\beta_\sigma} \\ \Delta_{21} = \coth\beta_k l+\frac{\beta_k}{8\alpha_a}\left(\frac{\alpha_k}{\beta_{a1}}+\frac{\tanh\beta_{a2}c}{\beta_{a2}}\right)+\frac{\beta_k}{2\beta_\sigma}; \qquad \Delta_{22} = -\frac{\beta_k}{8\alpha_a}\left(\frac{\alpha_k}{\beta_{a1}}+\frac{\tanh\beta_{a2}c}{\beta_{a2}}\right)-\frac{\beta_k}{2\beta_\sigma} \\ \Delta_b = 1+\frac{\beta_k^2c^2}{8\alpha_a(1+t_a/t_1)}\left[\frac{\beta_{a2}c\coth\beta_{a2}c-1}{\beta_{a2}^2c^2}-\frac{(\beta_{a1}c-1)}{\beta_{a1}^2c^2}\right] \end{cases} \tag{48}$$

IV. Numerical Results and Discussion

Geometrically nonlinear finite element analyses were conducted using MSC/NASTRAN for the single-strap model with isotropic and composite adherends shown in Fig. 1a. The following geometrical parameters are used: $t_1 = 1.6$ mm, $t_a = 0.2$ mm, ply thickness is 0.2 mm, $c/t_1 = 16$, and $l/c = 5$. It is worth noting that the parameter $c/t_1 = 16$ represents a relatively long overlap. The material properties of each individual ply in the composite adherends are $E_{11} = 138$ GPa, $E_{22} = E_{33} = 9.4$ GPa, $\nu_{12} = \nu_{13} = \nu_{23} = 0.32$, $G_{12} = G_{13} = 6.7$ GPa, and $G_{23} = 3.56$ GPa. The material properties for the isotropic adherends are taken as $E = 70$ GPa and $\nu = 0.3$. The adhesive properties are assumed to be $E_a = 2.4$ GPa and $\nu_a = 0.4$. The two types of layups used for the composite adherends are $[0/90/0/90]_s$ (referred to as C_0 with a surface ply of 0 deg hereafter) and $[90/0/90/0]_s$ (referred to as C_{90} with a surface ply of 90 deg hereafter).

For the purpose of comparison, $(\beta_k c)_{\max} = 8$ is chosen for the repair model with three different adherends. When $\beta_k c = 8$, the corresponding tensile loads per unit width are 641, 821, and 416 N/m, respectively, for the repair models with isotropic adherends, the C_0 and C_{90} composite adherends, and the chosen parameters. The associated average longitudinal stress of the outer adherend can be calculated and they are 401, 513, and 260 MPa, respectively.

In the NFEA, the meshing scheme includes the following:

1) Two and three elements were used through the thickness of each ply and adhesive layer in the regions of $0.7c \le |x| \le c$, and the element length is 0.1024 mm (or $0.004c$) along the axis in the regions.

2) One element was used across the thickness of each ply and adhesive layer in the region of $-0.65c \le x \le 0.65c$.

3) Graded mesh was used in the regions of $0.65c \le |x| \le 0.7c$. The 2D plane strain NFEA for the composite adherends was modeled using the bulk data entry MAT2 of MSC/NASTRAN.

For the purpose of simplification in presenting the numerical results, we use the abbreviations NFEA, F-Sol, and S-Sol to represent the results predicted by the geometrically nonlinear finite element analysis, the present full solutions presented in Sec. II, and the simplified solutions given in Sec. III. In all figures, the following definitions are used:

$$\xi = \frac{x}{c}; \qquad w_{n1} = \frac{w_1}{t_1}; \qquad w_{n\rm I} = \frac{w_1(-c)}{t_1}; \qquad w_{n\rm II} = \frac{w_2(+c)}{t_1}$$
$$\text{diff} = \frac{|w_{\rm NFEA}-w_{\rm full}|}{|w_{\rm NFEA}|}\cdot 100 \tag{49}$$

The subscripts NFEA and full in Eq. (49) indicate the results predicted by using the geometrically nonlinear finite element analyses and the present full solutions.

A. Overlap Deflection and Highly Nonlinear Behavior

Figures 3–5 depict the deflection curves of adherend 1 in the overlap for the single-strap model with isotropic adherends and composite adherends with layups of $[0/90/0/90]_s$ (C_0) and $[90/0/90/0]_s$ (C_{90}), respectively. The maximum differences between the NFEA and the present full solution occur at $x = -c$, for which the values for the considered three types of adherends cases are 2.04, 8.42, and 8.25%, respectively; the differences at $x = c$ are 1.86, 4.05, and 5.97%, respectively. Figures 3–5 show that there is a very good agreement between the results predicted using the NFEA and the present solutions. It is noted that the maximum deflections predicted by the NFEA are $0.773t_1$, $0.883t_1$, and $0.814t_1$ for the cases of three types of adherends in the repair model of Fig. 1a. This also indicates that the adherend deflections are considerably large.

Figure 6 illustrates the loading-deflection curves predicted by the geometrically nonlinear finite element analysis and the present solutions for the composite adherends with a layup of $[90/0/90/0]_s$ (C_{90}). In this figure, the applied longitudinal load is $F_{(C_{90})\max} = 416$ N/mm. For the other two cases, similar curves can also be obtained. The maximum relative difference of $w_{n\mathrm{II}}[=w_2(+c)/t_1]$ between the NFEA and the present full solution is less than 9%, as shown in Fig. 6 for the considered example.

Figures 3–6 also show that the present simplified solutions represent amazingly precise approximations of the full analytical solutions. It is also shown that the differences in adherend deflections calculated by the analytical solutions for the repairs with composite adherends are slightly larger than those with isotropic adherends, but the present analytical solutions are sufficiently accurate for engineering applications for both isotropic and composite single-strap models shown in Fig. 1a.

The loading-deflection curves in Fig. 6 depict the highly nonlinear behaviors of the model for the single-sided bonded composite patch repair to cracked structures. By referring to the comparison of the large deflections in Figs. 3–6 and the nonlinear relations in Fig. 6, it is clear that the present closed-form solutions capture the essential nonlinear features of the single-strap repair model.

B. Edge-Moment Factors

When deflections $w_3(l)$, $w_1(-c)$, and $w_2(+c)$ are obtained from the NFEA computation using MSC/NASTRAN, the edge-moment factors predicted by the NFEA are defined as

$$k_{\mathrm{I}} = -\frac{w_3(l)}{t_1 + t_a} = -\frac{w_1(-c)}{t_1 + t_a} = -\frac{w_{\mathrm{I}}}{t_1 + t_a}$$
$$k_{\mathrm{II}} = \frac{t_1 + t_a + w_2(+c)}{t_1 + t_a} = \frac{t_1 + t_a + w_{\mathrm{II}}}{t_1 + t_a} \tag{50}$$

Equation (50) is derived by using Eqs. (1), (37), and (40). For the single-sided bonding patch repair model with isotropic adherends and C_0 composite adherends, the edge-moment factors are depicted in Figs. 7 and 8. For the C_{90} composite adherends, the edge-moment factors are not presented because the $w_{n\mathrm{I}}$ and $w_{n\mathrm{II}}$ are plotted in Fig. 6. Figures 7 and 8 show that there is a good agreement among the present analytical solutions, the present simplified solutions, and the geometrically nonlinear finite element analysis for the edge-moment factors k_{I} and k_{II} for the bonded patch repair models with isotropic and composite adherends.

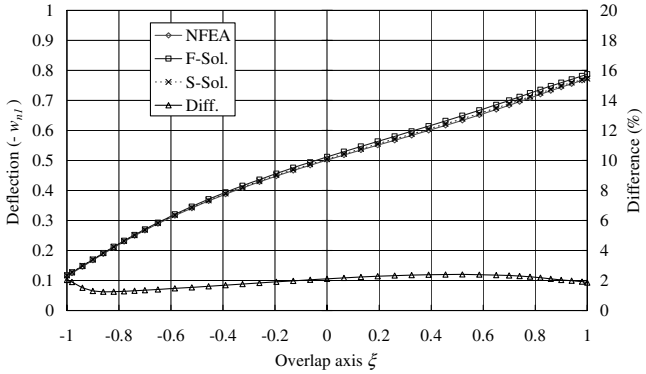

Fig. 3 Comparison among the adherend deflections in the overlap predicted by geometrically nonlinear finite element analysis, the present full and simplified solutions for the repair model with isotropic adherends at $\beta_k c = 8$.

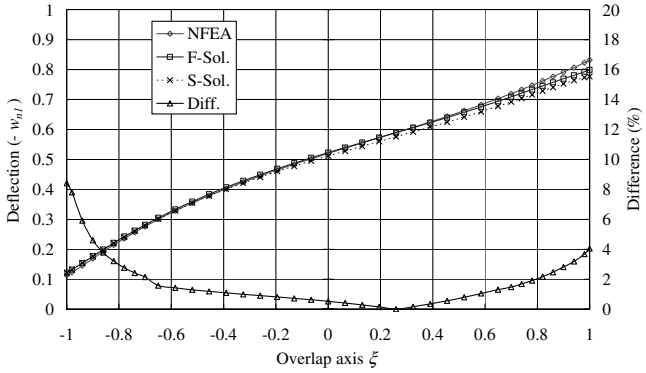

Fig. 4 Comparison among the adherend deflections in the overlap predicted by geometrically nonlinear finite element analysis, the present full and simplified solutions for the composite repair model with a layup of $[0/90/0/90]_s$ (C_0) and $\beta_k c = 8$.

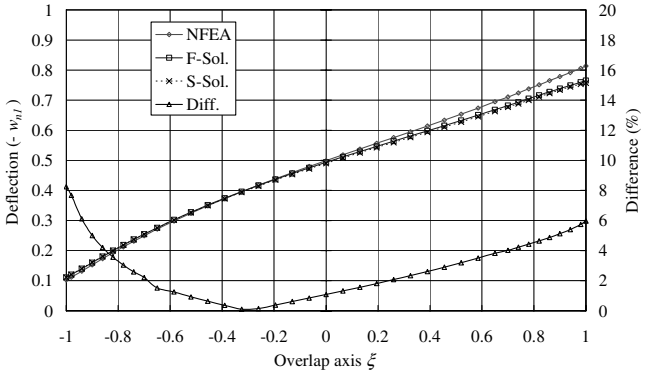

Fig. 5 Comparison among the adherend deflections in the overlap predicted by geometrically nonlinear finite element analysis, the present full and simplified solutions for the composite repair model with a layup of $[90/0/90/0]_s$ (C_{90}) and $\beta_k c = 8$.

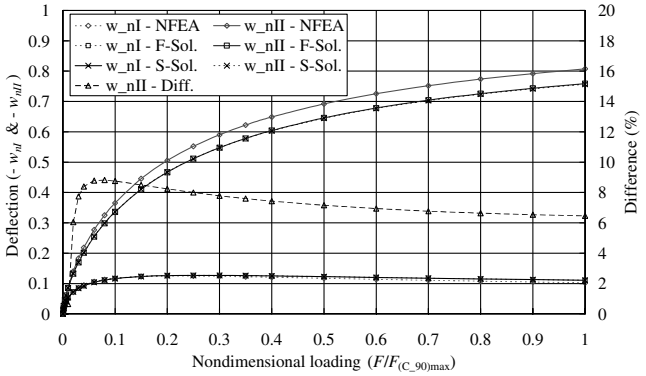

Fig. 6 Curves of the nondimensionalised tensile load ($F/F_{(C_{90})\max}$) and deflections (w_{nI} & w_{nII}) for a composite repair model with an adherend layup of $[90/0/90/0]_s$ (C_{90}).

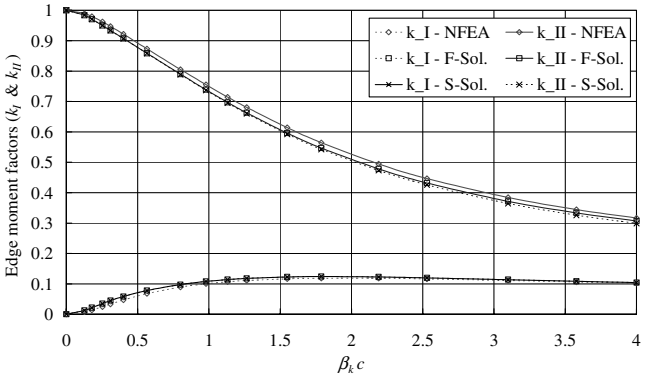

Fig. 7 Edge-moment factors predicted by the geometrically nonlinear finite element analysis, the present full and simplified solutions for the repair model with isotropic adherends.

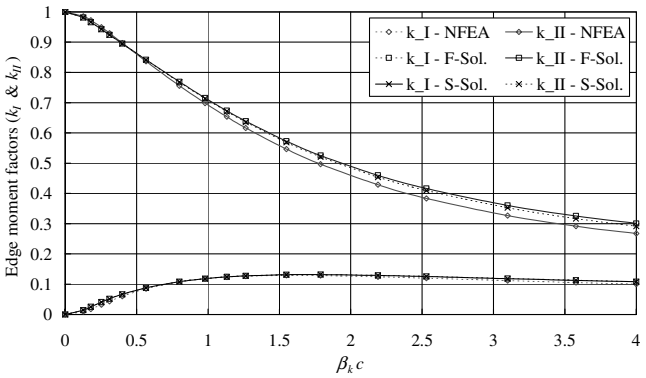

Fig. 8 Edge-moment factors predicted by the geometrically nonlinear finite element analysis, the present full and simplified solutions for the composite repair with an adherend layup of $[0/90/0/90]_s$ (C_0).

C. Adhesive Stresses

In the region of $-0.65c \le x \le 0.65c$, stresses τ_{xy} and σ_{yy} at the element center of the adhesive layer are used to represent shear and peel stresses, whereas in the regions of $(0.7c \le |x| \le c)$, stresses τ_{xy} and σ_{yy} at the element center of the three elements are averaged across the adhesive to determine the adhesive shear and peel stresses. The adhesive stresses in the transition regions of $0.65c \le |x| \le 0.7c$ are not used in Figs. 9–12.

Shear stress distributions of the repair models with composite adherends are given in Fig. 9. It can be seen that the shear stresses predicted by the present full solutions, and the present simplified solutions agree reasonably well with those predicted by the geometrically nonlinear finite element analyses using MSC/NASTRAN. In the regions near the adhesive ends $(0.95c \le |x|)$, the shear stresses predicted by the present formulations for the composite adherends with a 0-deg surface ply (C_0) are better than those for the composite adherends with a 90-deg surface ply (C_{90}). For example, the relative differences in shear stresses at $x = 0.994c$ predicted by the present full solution and the nonlinear finite element analyses are 15.5 and 32.2% for the cases of C_0 and C_{90}, respectively. This is believed to be primarily due to the lower extensional and transverse stiffness of the 90-deg surface ply (C_{90}) compared with the 0-deg surface ply (C_0).

Figures 10 and 11 depict the adhesive peel stresses for the repair models with C_0 and C_{90} composite adherends. Unlike the correlations of the deflection, edge-moment factors, and shear stress, there is a less favorable correlation between the peel stress predicted by the present formulations and the NFEA, especially in the peak values. For example, the peel stresses for the C_0 and C_{90} composite adherend cases at $x = 0.998c$ have a relative difference of 17.6 and 30%, respectively. It is believed that this is due to the influence of the lower transverse and extensional stiffness of a composite adherend compared with its longitudinal stiffness, which is not considered in the present formulation but is fully modeled in the geometrically nonlinear finite element analyses. This indicates that it becomes important to employ higher-order theory of modeling adhesive layer and stresses (Frostig et al. [14], Mortensen and Thomsen [15], and Luo and Tong [16]). It is also well known that the through-thickness stress prediction of laminates using the classical beam theory is generally poor. Fortunately, the present formulations employing the Euler beam theory accurately predict the large deflection, edge-moment factors, and shear stress for the repair model with composite adherends. Thus, it is adequate to neglect the higher-order terms given in Eq. (8), and the present analytical solutions describe the key characteristics of the bonded composite patch repair model.

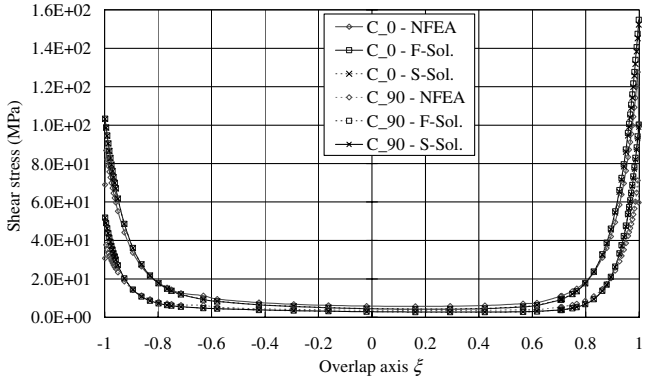

Fig. 9 Shear stress distributions predicted by the geometrically nonlinear finite element analysis, the present full and simplified solutions for composite repairs with adherend layups of $[0/90/0/90]_s$ (C_0) and $[90/0/90/0]_s$ (C_{90}).

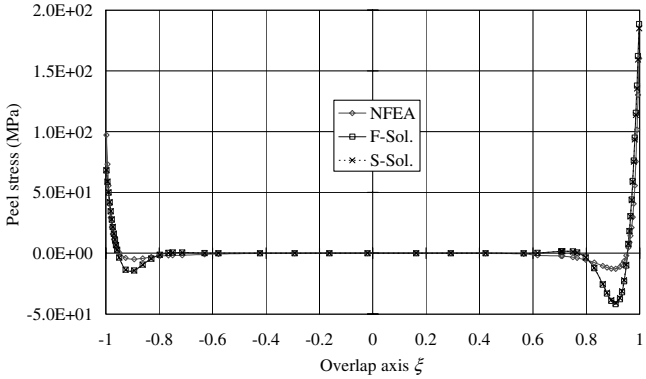

Fig. 10 Peel stress distributions predicted by the geometrically nonlinear finite element analysis, the present full and simplified solutions for the composite repair with an adherend layup $[0/90/0/90]_s$ (C_0).

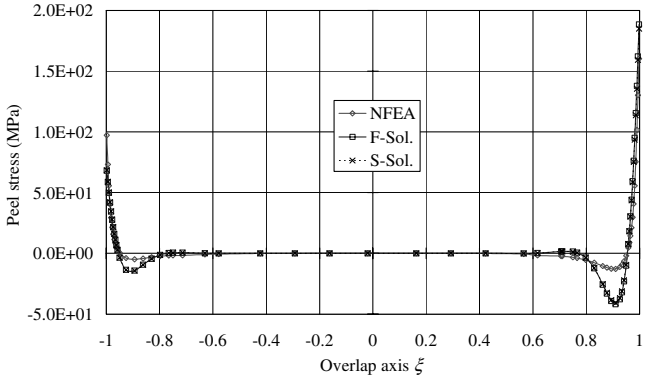

Fig. 11 Peel stress distributions predicted by the geometrically nonlinear finite element analysis, the present full and simplified solutions for the composite repair with an adherend layup of $[90/0/90/0]_s$ (C_{90}).

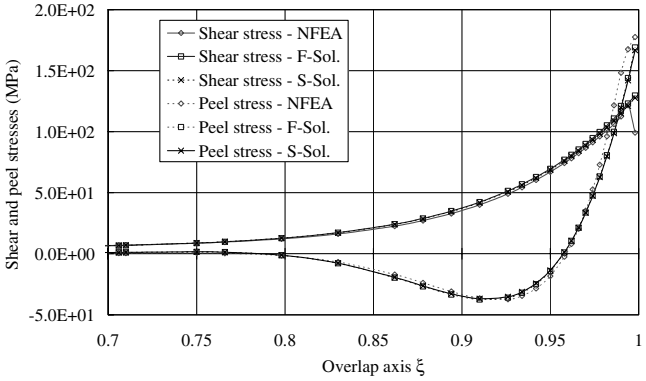

Fig. 12 Shear and peel stress distributions predicted by the geometrically nonlinear finite element analysis, the present full and simplified solutions for the repair model with isotropic adherends.

For the repair model with isotropic adherends, shear and peel stresses predicted by the present full solutions and the simplified solutions correlate extremely well with those predicted by the NFEA, as shown in Fig. 12. For adhesive peel stress, the remarkable correlation shown in Fig. 12 reflects a contrast to the less favorable correlation in Figs. 10 and 11. This comparison reveals that the adhesive strain definitions in Eq. (5) are more adequate for analyzing bonded metallic joints and repairs, and it also shows that it is important and necessary to modify the adhesive strain definitions in Eq. (5) for analyzing bonded composite joints and repairs.

V. Conclusions

The salient points of the present paper include: 1) development of the mathematically admissible governing equations based on the geometrically nonlinear analysis for the considered single-strap repair model with isotropic and composite adherends; 2) development of closed-form analytical full solutions and their simplifications for adherend displacements, edge-moment factors and adhesive stresses that account for all the geometrical and material parameters as well as the feature of large deflections; 3) validation of the present full and simplified solutions for adherend deflections, edge-moment factors, and adhesive stresses for the cases with both isotropic and composite adherends via comparing with the results predicted by using the geometrically nonlinear finite element analyses; and 4) confirmation of the adequacy of present governing equations and their solutions, including their simplifications, in terms of capturing the feature of large deflections of the overlap and the outer adherend.

Acknowledgment

The authors are grateful for the support of the Australian Research Council via Discovery-Projects grant DP0666683.

References

[1] Baker A. A., and Jones R. (ed.), *Bonded Repair of Aircraft Structures*, Martinus Nijhoff, New York, 1988.

[2] Baker, A. A., "Fiber Composite Repair of Cracked Metallic Aircraft Components: Practical and Basic Aspects," *Composites*, Vol. 18, No. 4, 1987, pp. 293–308. doi:10.1016/0010-4361(87)90293-X

[3] Wang, C. H., Rose, L. R. F., and Callinan, R., "Analysis of Out-Of-Plane Bending in One-Sided Bonded Repair," *International Journal of Solids and Structures*, Vol. 35, No. 14, 1998, pp. 1653–1675. doi:10.1016/S0020-7683(97)00129-7

[4] Belhouari, M., Bouiadjra, B. B., Megueni, A., and Kaddouri, K., "Comparison of Double and Single Bonded Repairs to Symmetric Composite Structures: A Numerical Analysis," *Composite Structures*, Vol. 65, No. 1, 2004, pp. 47–53. doi:10.1016/j.compstruct.2003.10.005

[5] Klug, J. C., and Sun, C. T., "Large Deflection Effects of Cracked Aluminum Plates Repaired with Bonded Composite Patches," *Composite Structures*, Vol. 42, No. 3, 1998, pp. 291–296. doi:10.1016/S0263-8223(98)00018-X

[6] Chalkley, P., and Baker, A., "Development of a Generic Repair Joint for Certification of Bonded Composite Repairs," *International Journal of Adhesion and Adhesives*, Vol. 19, Nos. 2–3, 1999, pp. 121–132. doi:10.1016/S0143-7496(98)90028-8

[7] Osnes, H., and Andersen, A., "Computational Analysis of Geometric Nonlinear Effects in Adhesively Bonded Single Lap Composite Joints," *Composites, Part B*, Vol. 34, No. 5, 2003, pp. 417–427. doi:10.1016/S1359-8368(03)00023-4

[8] Oterkus, E., Barut, A., Madenci, E., and Ambur, D. R., "Nonlinear Analysis of a Composite Panel with a Cutout Repaired by a Bonded Tapered Composite Patch," *International Journal of Solids and Structures*, Vol. 42, Nos. 18–19, 2005, pp. 5274–5306. doi:10.1016/j.ijsolstr.2005.02.024

[9] Kaye, R., and Heller, M., "Finite Element-Based Three-Dimensional Stress Analysis of Composite Bonded Repairs to Metallic Aircraft Structure," *International Journal of Adhesion and Adhesives*, Vol. 26, No. 4, 2006, pp. 261–273. doi:10.1016/j.ijadhadh.2005.03.016

[10] Luo, Q. T., and Tong, L. Y., "Fully-Coupled Nonlinear Analysis of Single Lap Adhesive Joints," *International Journal of Solids and Structures*, Vol. 44, Nos. 7–8, Apr. 2007, pp. 2349–2370. doi:10.1016/j.ijsolstr.2006.07.009.

[11] Krenk, S., "Energy Release Rate of Symmetric Adhesive Joints," *Engineering Fracture Mechanics*, Vol. 43, No. 4, 1992, pp. 549–559. doi:10.1016/0013-7944(92)90198-N

[12] Tong, L. Y., and Steven, G. P., *Analysis and Design of Structural Bonded Joints*, Kluwer Academic, Boston, 1999.

[13] Goland, M., and Reissner, E., "The Stresses in Cemented Joints," *Journal of Applied Mechanics*, Vol. 11, Mar. 1944, pp. A17–A27.

[14] Frostig, Y., Thomsen O. T., and Mortensen, F., "Analysis of Adhesive-Bonded Joints, Square-End, and Spew-Fillet: High-Order Theory Approach," *Journal of Engineering Mechanics*, Vol. 125, No. 11, 1999, pp. 1298–1307. doi:10.1061/(ASCE)0733-9399(1999)125:11(1298)

[15] Mortensen, F., and Thomsen, O. T., "Analysis of Adhesive Bonded Joints: A Unified Approach," *Composites Science and Technology*, Vol. 62, Nos. 7–8, 2002, pp. 1011–1031. doi:10.1016/S0266-3538(02)00030-1

[16] Luo, Q. T., and Tong, L. Y., "Linear and Higher Order Displacement Theories for Adhesive Bonded Lap Joints," *International Journal of Solids and Structures*, Vol. 41, Nos. 22–23, 2004, pp. 6351–6381. doi:10.1016/j.ijsolstr.2004.05.024

F. Pai
Associate Editor